Cyclic Loading of Beams Based on Kinematic Hardening Models: A Finite Element Approach

Ehsan Hashemi and Behrooz Farshi

***Abstract*—two major kinematic hardening models are employed in this article to study the behavior of Euler-Bernoulli beams by a finite element formulation of the plasticity problem. The proposed finite element formulation uses a variable stiffness matrix in each incremental step reflecting the yield surface movement. Moreover, complete formulation is presented for both load and deformation controlled cases. Examples are worked out for the Ziegler-Prager and the Armstrong-Frederick theories, to show the stress-strain behavior under cyclic symmetric and asymmetric flexural loading. The results have been graphically illustrated in plots of the stress-strain curves and are compared to the published and experimental ones. It was observed that Ziegler-Prager theory for isotropic cases with symmetric and asymmetric loading conditions. The presented simulation results confirm that the anisotropic cases with symmetric loading exhibit a ratcheting response. While the results show agreement with published ones; it was also observed that the two kinematic hardening theories do not show similar responses of reverse plasticity or ratcheting for Euler-Bernoulli beams in all the example cases.**

***Index Terms*— Classical beams, Cyclic loading, Kinematic hardening, Ratcheting, Reverse plasticity**

I. Introduction

Most studies in plasticity behavior of various elements have been carried out based on isotropic and kinematic hardening approaches. Hardening of any engineering material under plastic deformation is an indication that yield function F is not invariable, but is a function of stress tensor components σ_{ij} and strains as well as loading history and path [1]. Ueda and Yamakawa proposed a yield function in [2] without the effect of creep $\dot{\bar{\varepsilon}}$. Materials which possess hardening quality require an increase in the applied stresses in order to undergo additional plastic deformations. This behavior is a result of changes in the plastic potential function as described in [3] and [4]. It has conclusively been shown that the yield function can be expressed as variables such as temperature, strain rate or creep, and applied stress, as well as work hardening parameter K which is in turn a function of plastic strains [5], [6], [7]. Several experimental results and analytical approaches confirm that the differential of plastic strain $d\varepsilon_{ij}^{p}$ is directly proportional to the differential of the plastic potential function as follow in case of no yield surface movement:

$$d\varepsilon_{ij}^{p} = d\lambda \frac{\partial F(\sigma_{ij})}{\partial \sigma_{ij}} = d\lambda S_{ij} \tag{1}$$

In which $d\lambda$ is a scalar and could be experimentally determined. This value is also subject to change during the loading process and related to the equivalent plastic strain and effective stress. Differential plastic strain in case of the yield surface movement is mathematically described as (2)

$$d\varepsilon_{ij}^{p} = \frac{3 d\varepsilon_{eq}^{p}}{2\sigma_{eq}}(S_{ij} - a_{ij}) \tag{2}$$

In (2) S_{ih}, a_{ij} are stress and back stress deviatoric tensors respectively [8] and [9]. Several hardening theories are available as presented in [10] and [11] for the movement of yield surface and plastic characteristics of materials among which Ziegler-Prager and the Armstrong-Frederick are the most practiced ones. Prager expressed a hardening theory [12], which with Ziegler's modification [13], forms a hardening law that has found wide applications. Armstrong-Frederick argued for a yield surface movement scheme in [14] depending on material properties in which total plastic strain in the previous load step calculations is accumulated and considered. This model is practically studied in [15] and [16] and employed in the presented paper as a kinematic hardening model. Under cyclic loading, when the accumulated total deformation results in strains larger than certain limits, a phenomenon known as ratcheting occurs. Ratcheting behavior leads to eventual structural breakdown as related investigations in [17] and [18] substantiate this matter from different aspects and diverse loading conditions. In anisotropic material tests under cyclic loading, one of the causes of ratcheting is the different behavior of material in tension and compression, which is numerically simulated here in section IV for the variable stiffness matrix of the beam finite element model. This procedure is introduced when there is a difference between material's strain hardening curves in tension and compression tests. On the other hand, when the net complete cycle total deformation is zero, reverse plasticity occurs as presented in this article for various flexural loading conditions. This paper has been divided into four sections. The first section deals with introduction of plasticity, cyclic loading, and kinematic hardening theory. Succeeding sections focuses on finite element modeling of the classical beams, thermo elastic-plastic stress analysis of beams, and numerical simulation of the proposed method respectively followed by discussion and conclusion.

Manuscript received April 20, 2011; revised July 6, 2011.

Ehsan Hashemi is with the Department of Industrial and Mechanical Engineering, Islamic Azad University, Qazvin Branch, Qazvin, Iran. (e-mail: e.hashemi@qiau.ac.ir).

Behrooz Farshi is with the Department of Mechanical Engineering, Iran University of Science and Technology, Narmak, Tehran, Iran. (e-mail: farshi@iust.ac.ir).

II. Finite Element Model of the Euler-Bernoulli Beams

This chapter describes the finite element modeling and characterization of classical beams and associated stiffness matrix definition. Classical beams theory assumes plane sections perpendicular to the beam axis, remain plane and perpendicular to it as described in [19]. As a result, displacement components can be written as:

$$u(x,y) = -y\frac{\partial w(x)}{\partial x}; v = -z\frac{\partial w}{\partial y}; w(x,y) = w(x) \tag{3}$$

Consider a beam element with four degrees of freedom under shear and bending actions. Beam element displacement is related with element shape functions $[N^e]$ and nodal displacements $\{U^e\}$ as shown in (4).

$$W^{(e)} = < N_{2i-1} \;\; N_{2i} \;\; N_{2j-1} \;\; N_{2j} > \begin{Bmatrix} w_{2i-1} \\ \theta_{2i} \\ w_{2j-1} \\ \theta_{2j} \end{Bmatrix} = < N^e > \{U^e\} \tag{4}$$

Shape functions in the above equation are specified by boundary conditions implementation. Assuming distributed load $\{q(x)\}$, boundaries s where the forces are applied, and body forces $\{X\}$ acting on the element, the $\{f^{(e)}\}$matrix is mathematically described in (5) and can be simplified further to the following form with the assumption of linear element and normally distributed load.

$$\{f^{(e)}\} = \int\int\int [N]^T \{X\} dV + \int_s \int [N^s]^T \{q\} dS = \int_0^l [N]^T \{q\} dx \tag{5}$$

Moreover, equilibrium equation takes the following form, in which $[C]$ represents the matrix of elastic moduli, in one, two, or three dimensional forms whichever the case may be. This results into the relation between assembled general stiffness matrix, deformations and load matrix as identified in [20].

$$\{f^{(e)}\} = \int\int\int [B]^T [C][B] dV \{U\} = [K_e]\{U\} \tag{6}$$

In which $[K_e]$ is the stiffness matrix for the beam element and will be variable in the elastic-plastic region.

III. Elastic-plastic stress analysis

This section deals with Elastic-Plastic stress analysis of elements and implementation of kinematic hardening phenomena in associated matrix solutions. Elastic-plastic stiffness matrix for each element is obtainable by applying variational methods to minimize the potential energy. It is numerically demonstrated in (7).

$$[K_e] = \int_V [B]^T [C_{eP}][B] dv \tag{7}$$

Elastic-plastic modulus $[C_{ep}]$ is employed for determination of each element's stiffness matrix. The differential thermal load which is a function of the thermal effects, strain-rate-dependent material properties, and differential mechanical load expression are employed to assemble the load matrix. Displacements of each element and element strains are then computed using shape functions. Element strains are executed to define stresses thru the constitutive relations. Convergence of the computed displacement in each increment is checked versus the assumed criterion and the step is repeated if necessary.

This section can best be treated under two headings: derivation of elastic-plastic stiffness matrix and kinematic hardening model assumption.

A. Elastic-plastic stiffness matrix

As previously stated, yield function can be expressed as a function of variables such as temperature, strain rate or creep, and applied stress, as well as work hardening parameter K which is in turn a function of plastic strains

$$F = F(\{\sigma\}, K, T, \bar{\dot{\varepsilon}}) \tag{8}$$

The observed correlation between plastic potential function and the above mentioned parameters in (8) results in dependency of element's elastic-plastic deformation to temperature changes, and strain rate of $\bar{\dot{\varepsilon}}$ as stated in (1). The following clause focuses on elastic-plastic modulus calculation to be employed in elements' variable stiffness matrix (7). Assembled stiffness matrix for the generalized form of analysis leads to calculation of displacements and total strain components successively. Effects of kinematic or isotropic hardening, temperature, and strain rate must also be taken into account for estimation of plastic potential function as stated in [21] and [22]. Therefore, chain differentiated form of plastic potential function results in:

$$dF = \left\{\frac{\partial F}{\partial \sigma}\right\}^T \{d\sigma\} + \frac{\partial F}{\partial K} dK + \frac{\partial F}{\partial T} dT + \frac{\partial F}{\partial \bar{\dot{\varepsilon}}} d\bar{\dot{\varepsilon}} \tag{9}$$

Since the hardening parameter K, indicates the plastic work done on the solid while the plastic deformation takes place, the second term of right hand of (9) can be written in terms of the plastic strain $\{d\varepsilon_P\}$. This term is computed from the following relationship:

$$\frac{\partial F}{\partial K} = \frac{\partial}{\partial K}\left(J_2 - \frac{1}{3}(\sigma_{eq})^2\right) = -\frac{2}{3}\sigma_{eq}\frac{\partial \sigma_{eq}}{\partial K} \tag{10}$$

Second deviatoric stress invariant J_2 and equivalent stress σ_{eq} are introduced in (10) for estimation of plastic potential function variation respect to the hardening parameter. On the other hand, $\frac{\partial \sigma_{eq}}{\partial K}$ is obtainable from the work done dK on the element undergoing plastic deformation based on the plastic strain energy as:

$$\frac{\partial \sigma_{eq}}{\partial K} = \frac{\partial \sigma_{eq}}{\partial \varepsilon_{eq}^P}\frac{d\varepsilon_{eq}^P}{dK} = H\frac{1}{\sigma_{eq}} = \frac{H}{\sigma_{eq}} \tag{11}$$

Thermo-elastic-plastic differential strains in a solid are expressed in (12):

$$\{\delta\varepsilon\} = \{\delta\varepsilon_e\} + \{\delta\varepsilon_{e,T}\} + \{\delta\varepsilon_{e,\dot{\varepsilon}}\} + \{\delta\varepsilon_T\} + \{\delta\varepsilon_P\} \tag{12}$$

In which $\{\delta\varepsilon_e\}$ and $\{\delta\varepsilon_P\}$ are elastic and plastic strain components. $\{\delta\varepsilon_{e,T}\}$ and $\{\delta\varepsilon_{e,\dot{\varepsilon}}\}$ are material's strain change characteristics which are subject to creep and temperature. Matrix notation of the Hooke's law stress-strain relationship with consideration of plastic deformation is given as:

$$\{d\sigma\} = [C_e](\{d\varepsilon\} - \{d\varepsilon_{e,T}\} - \{d\varepsilon_{e,\dot{\varepsilon}}\} - \{d\varepsilon_T\} - \{d\varepsilon_P\}) \tag{13}$$

Elastic-plastic constitutive relation for each element is introduced in (14):

$$[C_{ep}] = [C_e] - [C_P] \tag{14}$$

In the above relation, matrix $[C_e]$ is the known elastic component, whiles the plastic part is related to both the yield function and elastic component as bellow:

$$[C_p]=\frac{1}{Sp}[C_e]\left\{\frac{\partial F}{\partial \sigma}\right\}\left\{\frac{\partial F}{\partial \sigma}\right\}^T[C_e] \tag{15}$$

In which:

$$Sp=\left\{\frac{\partial F}{\partial \sigma}\right\}^T[C_e]\left\{\frac{\partial F}{\partial \sigma}\right\}-\frac{\partial F}{\partial K}\left\{\frac{\partial K}{\partial \varepsilon_P}\right\}^T\left\{\frac{\partial F}{\partial \sigma}\right\} \tag{16}$$

Using expression (11) in (10) the term $\frac{\partial F}{\partial K}$ is determined. Thus the fundamental thermo-elastic-plastic relationship takes the following shape:

$$\begin{aligned}&\{d\sigma\}=[C_{eP}]\{d\varepsilon\}\\&-[C_{eP}]\left(\{\alpha\}dT+\frac{\partial[C_e]^{-1}}{\partial T}\{\sigma\}dT+\frac{\partial[C_e]^{-1}}{\partial \bar{\varepsilon}}\{\sigma\}d\bar{\varepsilon}\right)\\&-\frac{[C_e]\{S\}}{Sp}\left(\frac{\partial F}{\partial T}dT+\frac{\partial F}{\partial \dot{\varepsilon}}d\dot{\varepsilon}\right)\end{aligned} \tag{17}$$

For the purpose of analysis, the following equation known as *Ludwick* type of axial plastic stress-strain curve is considered.

$$\sigma=\sigma_Y+m{\varepsilon_p}^n \tag{18}$$

Variations in the partial plastic strain are contributed to the yield surface movement and related kinematic hardening models which will be described in the following subsection. This partial strain is essential for determination of elastic-plastic stress tensor as illustrated in (17).

B. Kinematic hardening model

Section II and the previous part of this section was introduced to lay out the theoretical dimensions of the finite element approach and also concentrates on taking out a reliable routine for elastic-plastic modulus determination without kinematic hardening assumption. Afterwards, this section is contributed to determination of partial yield surface movement and its correlation with the accumulated yield surface movement and stress tensor. *Bauschinger's* property indicates that in metals under cyclic loading, a strain hysteresis loop is exhibited [22] and [23]. This characteristic is employed in this research and the following equation shows relation between differential yield surface movement and current stress status

$$d\alpha_{ij}=d\mu(\sigma_{ij}-\alpha_{ij}) \tag{19}$$

Coefficient $d\mu$ is demonstrated as follows with tensor notation

$$d\mu=\left\{\frac{\partial F}{\partial \sigma_{ij}}d\sigma_{ij}+\frac{\partial F}{\partial T}dT+\frac{\partial F}{\partial \dot{\varepsilon}}d\dot{\varepsilon}\right\}\Big/\left\{(\sigma_{kl}-\alpha_{kl})\frac{\partial F}{\partial \sigma_{kl}}\right\} \tag{20}$$

As a consequence of the *Prager's* modified model, the following equation represents numerical description of the yield surface movement respect to the plastic differential strains

$$d\alpha_{ij}=C(T,\dot{\varepsilon})d\varepsilon_{ij}^P \tag{21}$$

In which α_{ij} is the yield surface movement tensor, $C(T,\dot{\varepsilon})$ is a property of the material obtainable from its stress strain curve [24] and $d\varepsilon_{ij}^P$ is the plastic strain component. Thus the plastic potential function F must be corrected to take into consideration the yield surface movement in the hardening behavior of the material. Such correction is performed in the stiffness matrix of the elements in each step of the finite element analysis process developed above. Employing elastic-plastic modulus $[C_{ep}]$ in the variable stiffness matrix containing loading history and plastic deformations has been characterized as an influential parameter for fast estimation of plastic deformations in each loading step satisfying convergence criteria. In the modified *Prager* rule, coefficients C, and H are obtained from a unidirectional test by the following equations:

$$C=\frac{d\alpha_x}{d\varepsilon_x^p};\ H=\frac{d\sigma_x}{d\varepsilon_x^p} \tag{22}$$

The quantities C and H used in each finite element solution step would be variable due to H and must be computed for each load step. Then the stress differential in each step of the solution process, and for every element can be computed from (17). The accumulation of such stress differentials leads to the stress strain variations which are exhibited as plots in the *Results and Discussion* section. In case of the *Armstrong-Fredrick* theory, a similar approach is undertaken [25]. In this case the movement of the yield surface is computed from the following:

$$d\alpha_{ij}=Cd\varepsilon_{ij}^p-\gamma\alpha_{ij}\left|d\varepsilon_{eq}^p\right| \tag{23}$$

In the above relation γ, C are material constants for this model obtainable from the uniaxial strain-controlled hysteresis curve. All the steps outlined for the modified *Ziegler-Prager* approach to find the expression for movement of yield surface can be repeated for this theory in a similar manner. The C quantities for each loading or unloading iteration cycle of the *Armstrong-Fredrick* model are obtained from H depending on the sign of $d\varepsilon_x^p$. For positive $d\varepsilon_x^p$, it is calculated by $H+\gamma\alpha_x$ and for negative $d\varepsilon_x^p$ in unloading it is $H-\gamma\alpha_x$.

Disadvantages of the presented approach for matrix estimations can be discussed under two headings, which are: large accumulated errors produced by high orders of stress values and low speed of tensor calculation for each load step. This drawback could be omitted by implementation of lower order values for stress and back stress tensors with normalization. In order to reduce the numerical order of stresses and strains in iterations, dimensionless quantities are introduced to enhance the accuracy and improve the rate of convergence. The dimensionless differential plastic strain and stress are normalized with respect to the yield strain and stress respectively as demonstrated in (24).

$$de_{ij}^p=\frac{d\varepsilon_{ij}^p}{\varepsilon_Y};d\sigma_{dij}=\frac{d\sigma_{ij}}{\sigma_Y} \tag{24}$$

Therefore, normalized differential plastic strain tensor according to the yield surface movement can be expressed as:

$$de_{ij}^p=\frac{3}{2}de^p(S_{dij}-a_{dij}) \tag{25}$$

In which a_{dij} is dimensionless back stress deviatoric

tensor. Normalized translated stress tensor $\{\sigma_d^*\}$, calculated by $\{\sigma_d\}-\{\alpha_d\}$ and translated deviatoric stress tensors $\{\bar{\sigma}_d^*\}$, which could be explained by $\{\sigma_d^*\}-\{\sigma_{dm}\}$ are used to get the normalized variable elastic-plastic stiffness matrix.

$$[C_d^{ep}]=[C_d^e]-6E[C_d^e]\{\bar{\sigma}_d^*\}\{\bar{\sigma}_d^*\}^T[C_d^e]/Sp_d \tag{26}$$

Sp_d appears in dimensionless form of its original expression in (27) which is now computed using the normalized elastic stiffness matrix, modulus of elasticity, dimensionless stresses, and deviatoric stresses in each increment.

$$Sp_d=6\{\bar{\sigma}_d^*\}^T\{\bar{\sigma}_d^*\}C+6E\{\bar{\sigma}_d^*\}^T[C_d^e]\{\bar{\sigma}_d^*\} \tag{27}$$

The dimensionless form of the yield surface movement in the two above mentioned kinematic hardening models, *Ziegler-Prager* and *Armstrong- Fredrick*, can be expressed as follows respectively:

$$d\alpha_{dij}=\frac{C_A}{E}de_{ij}^p \tag{28}$$

$$\begin{aligned}d\alpha_{dij}&=\frac{C_A}{E}de_{ij}^p-\gamma\alpha_{dij}\left|de_{ij}^p\right|\varepsilon_Y\\&=6C_A\bar{\sigma}_{dij}^*d\lambda-\gamma\alpha_{dij}\left|de_{ij}^p\right|\varepsilon_Y\end{aligned} \tag{29}$$

Various loading conditions such as deformation controlled and flexural loading controlled, and their effects on the element behavior are discussed in the following section

IV. Results and Discussion

This study set out with the aim of variable stiffness matrix and employing dimensionless parameters to analyze the cyclic loading behavior of beams. This section provides results of the above mentioned approach for various loading conditions. The relevance of kinematic hardening models (*Ziegler-Prager* and *Armstrong-Frederick* in this article) is clearly supported by the current findings The following figures represent the axial stress-strain curves for two cases of deformation-controlled, and flexural load-controlled, for both yield surface movement theories namely *Prager*'s as modified by Ziegler, and the *Armstrong-Frederick's* on the classical beams. These results are checked against published results and some experimental tests for correctness.

The first set of analysis examined the effect of solution method on the elastic-plastic behavior of elements. Fig. 1 illustrates the correlation between solution methods with the plot of effective stresses versus axial strains. The flexural moment applied was 3400 N.m.

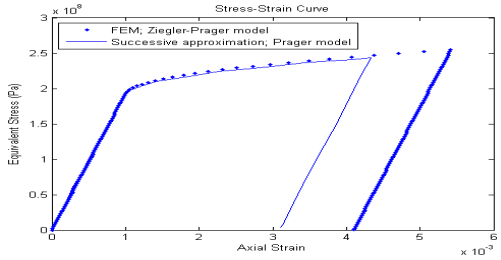

Fig. 1. Results of successive approximation method based on *Prager's* model and proposed FEM using *Ziegler-Prager* model.

Results are checked and compared with the plastic solution by the successive approximation method presented in [25]. m coefficient and n power in (18) for plastic strain are taken as $m=896Mpa$, $n=0.5$. Furthermore, the modulus of elasticity and yield stress are taken as $E=193\,Gpa$, $\sigma_y=193\ Mpa$. An implication of the finding from Fig. 1 is that the successive approximation method though using the unmodified *Prager* model indicates a lower axial strain in this case. Results for various kinematic hardening models including *Ziegler-Prager* and two *Armstrong-Frederick* schemes are graphically demonstrated in Fig. 2 which confirms uniformity of these methods within a specified strain margin.

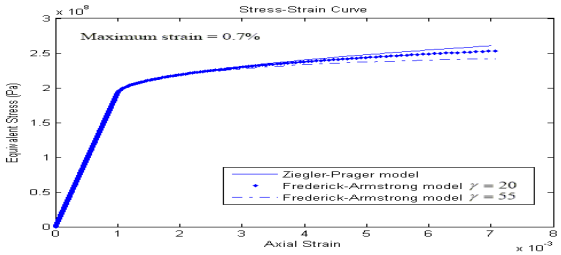

Fig. 2. Comparison of yield surface movement models.

As a consequence of implementing finite element method and variable stiffness matrix in this article, it appears that *Armstrong-Frederick's* method predicts lower equivalent stress which depends on the kinematic hardening characteristics. Fig. 3 demonstrates classical beam undergoing plastic stress. Loading is deformation controlled in the range of $0<\varepsilon_{total}<0.5\%$. Other physical characteristics of the two example beams as given in the figure are exactly alike.

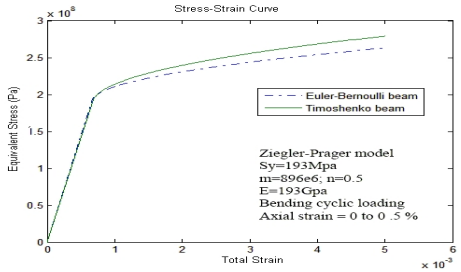

Fig. 3. Comparison of the behavior of Timoshenko beam with Euler-Bernoulli for strain controlled loading

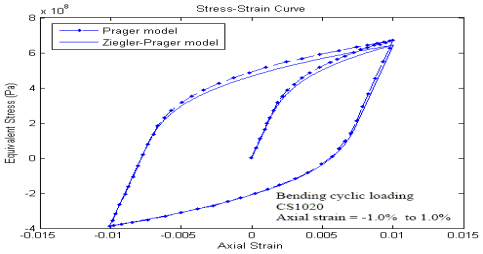

Fig. 4. Cyclic flexural loading with finite axial strain on *Euler-Bernoulli* beam; comparison of two models.

Fig. 4 depicts deformation controlled loading on EB beam representing two *Prager* models' results. These differences can be explained in part by proximity of two models except the *Ziegler* modifications mentioned in (17) and (18). These results are consistent with those of Hassan and Kyriakides

studies in [9] and suggest that both models exhibit revered plasticity. This experiment is performed on a CS1020 steel beam with $E = 173.2\ Gpa$, and yield stress of $\sigma_Y = 241 Mpa$, $m = 2631 Mpa$, $n = 0.35$ taken for the axial stress strain relation.

In Fig. 5 *Euler-Bernoulli* model undergoes cyclic flexural loading for two kinematic hardening models. Impose loading is employed to get axially asymmetric deformation $\varepsilon_x = -0.5\%\ to\ 0.1\%$ for the same CS1020 material. The mean axial strain is not zero, and the curve confirms reverse plasticity.

Fig. 6 shows the results for deformation controlled flexural loading with non-zero mean stress. Although the mean applied stress is non-zero, the stress strain curve suggests reverse plasticity behavior, which is consistent with the results in [25].

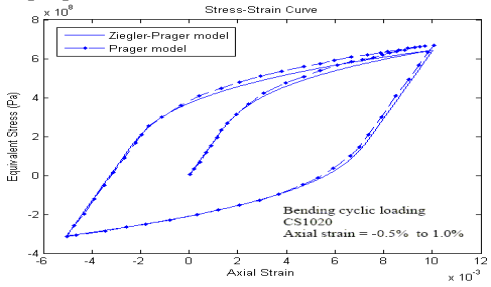

Fig. 5. Cyclic loading results on the beam with non-zero mean axial strain; comparison of *Prager's*, and its modified model.

Fig. 7 shows the results for flexural cyclic loading and unloading, using the modified *Prager* model with consideration of anisotropy in material property.

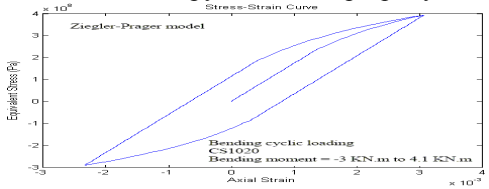

Fig. 6. Flexural loading on beam with non-zero mean stress.

In Fig. 7 there is a clear trend of strain due to anisotropy effect during cyclic loading which results in ratcheting.

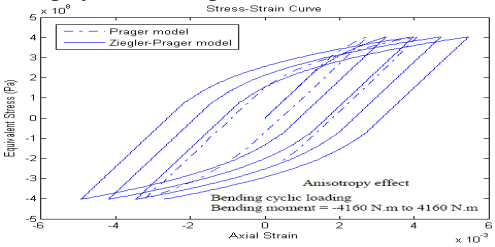

Fig. 7. Behavior of *Euler-Bernoulli* beam under cyclic flexural loading based on *Prager* and *Ziegler-Prager* models with material anisotropy.

The coefficients m, n are therefore different in loading and unloading, causing unequal slopes in the plastic zone. The values used for loading phase are $m = 2631\ Mpa$, $n = 0.35$, and for the unloading phase $m = 3136 Mpa,\ n = 0.37$. The stress strain curves in Fig. 7 are comparable to the curves in [25] and [26] for the axial cyclic loading with zero mean stress which indicates ratcheting behavior for the mentioned type of loading and the same material properties.

Fig. 8 shows the *Armstrong-Frederick* model under deformation controlled symmetric loading i.e. zero mean strain. In case of asymmetric flexural cyclic load application on an Euler-Bernoulli beam, using the *Armstrong-Frederick* yield surface movement theory, the finite element procedure used herein predicts a ratcheting behavior.

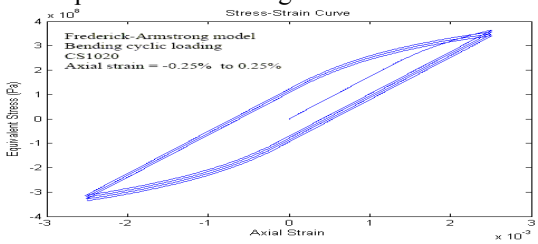

Fig. 8. Cyclic loading behavior for axial strain with zero mean, for a *Frederick-Armstrong* model .

Results for flexural loading on an *Euler-Bernoulli* beam with zero mean stress using *Armstrong-Frederick* yield surface movement model is shown in Fig. 9. The flexural loading is symmetric, and the results indicate a reversed plasticity behavior which is consistent with results of [20] and [25].

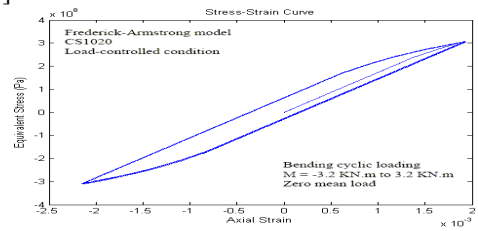

Fig. 9. Behavior of classical beam under symmetric cyclic loading.

In case of flexural stresses with non-zero mean, cyclic increase in the strains would ultimately cause failure of the beam.

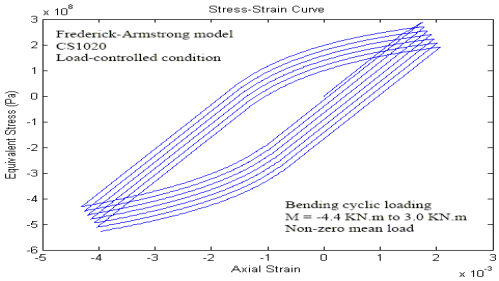

Fig. 10. Cyclic strain increase under asymmetric flexural loading based on *Armstrong-Frederick* yield surface movement model.

This can be illustrated briefly by ratcheting behavior in Fig. 10, and is compatible with the behavior predicted in [26] and [27].

V. Conclusions

Presented approach is studied on the beam element which shows a reasonable outcome with acceptable deviations during loading and unloading. In addition, the present findings seem to be consistent with other research on beam elements with other numerical methods such as successive approximations. The employed finite element method allows stiffness matrix to be subject to change due to the movement and changes in the yield surface per loading increment. As a consequence of implementing this matrix, it appears that elastic-plastic behavior of beam elements is properly

represented under thermal and mechanical loadings.

Proposed method results are compared with the result of successive approximations method and experimental results and were shown to be similar for the classical theory. The presented finite element method offers a practical modeling of beams behavior under cyclic loading for both hypotheses of *Ziegler-Prager* and *Armstrong-Frederick*. It is concluded that the *Ziegler-Prager* model predicts reverse plasticity for this type of beams under cyclic flexural loading in both cases of deformation and load controlled in symmetric and asymmetric loadings whereas, the same variable stiffness matrix technique in case of non-symmetric loading predicts a ratcheting behavior for the *Armstrong-Frederick* model.

Another important practical implication is that in cases of materials with anisotropic tension/compression curves, the finite element method predicts ratcheting behavior for *Ziegler-Prager* model. Moreover, dimensionless substitutes of stress and strain tensors are employed for fast convergence and reducing order of stress-strain and back stress values. The results show agreement with those predicted in [18], [20], [25], [26], and [30] for mechanical loadings.

Further experimental investigations are needed to estimate responses of higher order beams to the *Ziegler-Prager* and *Armstrong-Frederick* models and establish a correlation between finite yield surface movements for this type of elements which are under study by the authors.

VI. Acknowledgment

Valuable guidance and advice of Dr. M. Reza Eslami, professor of mechanical engineering at AmirKabir University of Technology, in this research work is hereby gratefully acknowledged.

References

[1] Chaboche JL, Time independent constitutive theories for cyclic plasticity. International Journal of Plasticity, 2, 149-88 (1986).

[2] Ueda, Y. and Yamakawa, T., Thermal nonlinear behavior of structures. In Advances in Computational Methods in Structural Mechanics and Design, J.T. Oden, R.W. Clough and Y. Yamamoto (eds.), pp. 375-392, University of Alabama Press, Huntsville, 1972.

[3] Argon AS, Ed., Constitutive Equations in Plasticity, MIT Press, Cambridge, Massachusetts, 1975.

[4] Chaboche, J.L. A review of some plasticity and viscoplasticity constitutive theories. International Journal of Plasticity, 24, 1642-1693 (2008).

[5] Slavik D and Sehitoglu H. Constitutive models for thermal loading. Journal of Engineering Materials and Technology, 108, 303-312 (1986).

[6] Hsu, T. R. The Finite Element Method in Thermomechanics, Allen & Unwin, Boston, 1990.

[7] Dowling, N. E., Mechanical Behavior of Materials, Second fedition, Prentice-Hall, NJ, 1998.

[8] Duszek, M. K. and Perzyna, P. On combined isotropic and kinematic hardening effects in plastic flow processes. International Journal of Plasticity, 7, 351-363 (1991).

[9] Corona, E., Hassan, T. and Kyriakides, S. On the performance of kinematic hardening rules in predicting a class of biaxial ratcheting histories. International Journal of Plasticity, 12, 117-145 (1996).

[10] Bari, S. Constitutive modeling for cyclic plasticity and ratcheting. Thesis submitted in partial fulfillment of the requirements for the degree of Doctor of Philosophy, January 2001.

[11] Chen, X. and Jiao, R. Modified kinematic hardening rule for multiaxial ratcheting prediction. International Journal of Plasticity, 20, 871-898 (2004).

[12] Prager, W. A. New method of analyzing stress and strains work-hardening plastic solids. Journal of Applied Mechanics, 23, 493-496 (1956).

[13] Ziegler, H. A modification of Prager's hardening rule. Applied Mathematics, 17, 55-65 (1959).

[14] Armstrong, P. J. and Frederick, C. O. A mathematical representation of the multiaxial Bauschinger effect, C.E.G.B Report No. RD/B/N 731, 1966.

[15] Jiang, Y. and Kurath, P. Characteristics of the Armstrong-Frederick type plasticity models. International Journal of Plasticity, 12, 387-415 (1996).

[16] Lubarda, V. A. and Benson, D.J. On the numerical algorithm for isotropic–kinematic hardening with the Armstrong–Frederick evolution of the back stress. Computer Methods in Applied Mechanics and Engineering, 191, 3583-3596 (2002).

[17] Rahmana, S. M., Hassana, T. and Coronab, E. Evaluation of cyclic plasticity models in ratcheting simulation of straight pipes under cyclic bending and steady internal pressure. International Journal of Plasticity, 24, 1756-1791 (2008).

[18] Hassana, T., Talebb L. and Krishnaa, S. Influence of non-proportional loading on ratcheting responses and simulations by two recent cyclic plasticity models. International Journal of Plasticity, 24, 1863-1889 (2008).

[19] Krishnamoorthy, C. S. Finite Element Analysis: Theory and Programming, Tata McGraw-Hill Publishing Company, New Delhi, 1987.

[20] Barham, W., Aref, A. and Dargush, G. On the elastoplastic cyclic analysis of plane beam structures using a flexibility-based finite element approach. International Journal of Solids and Structures, 45, 5688-5704 (2008).

[21] Owen, D. R. and Hinton, E. Finite Elements in Plasticity, Theory and Practice, Pineridge Press, New York, 1980.

[22] Zahavi, E. and Torbilo, V. Fatigue Design Life Expectancy of Machine Parts, CRC, Boca Raton, 1996.

[23] Jiang, Y. and Zhang, J. Benchmark experiments and characteristic cyclic plasticity deformation. International Journal of Plasticity, 24, 1481-1515 (2008).

[24] Crisfield, M. A. Non-Liner Finite Element Analysis of Solids and Structure, Edition, Vol. 2, John Wiley & Sons, Chichester, 1997.

[25] Eslami, M. R. and Mahbadi, H. Cyclic loading of beams based on the Prager and Frederick- Armestrong kinematic hardening models. International Journal of Mechanical Sciences, 44, 859-879 (2002).

[26] Hassana, T. and Kyriakides, S. Ratcheting in cyclic plasticity, Part 1; Uniaxial Behavior. International Journal of Plasticity, 8, 91-116 (1992).

[27] Lima, C. B., Kim, K. S. and Seonga, J. B. Ratcheting and fatigue behavior of a copper alloy under uniaxial cyclic loading with mean stress. International Journal of Fatigue, 31, 501-507 (2009).

Ehsan Hashemi,was born in Tehran, Iran, in 1979. He earned M.Sc degree in Mechanical Eng., applied design, at AmirKabir University of technology (formerly Tehran polytechnic), Tehran, Iran in 2005 and B.Sc in Mechanical Engineering at Iran University of Science and Technology, Tehran, Iran in 2002. He has more than 5 years of teaching experience and currently works as an lecturer at the Faculty of Industrial and Mechanical Engineering, Islamic Azad University, Qazvin Branch, and a researcher in the Mechatronics Research Laboratory, MRL on applied numerical methods, vibration, control, and FEM.

Mr. Hashemi has published more than 15 research papers in ASME and IEEE conference proceedings and international journals. His research interests include advanced computing, methods, optimization, FEM, vibration, dynamic simulation, and control.

Behrooz Farshi, has more than 25 years of teaching experience and currently works as an associate emeritus Prof. at the Department of Mechanical Engineering, Iran University of Science and Technology,

Prof. Farshi has published many research papers in international journals and ASME conference proceedings. His research interests are optimization of structural and mechanical systems, computational mechanics, eigen problems in stability & vibration.